Ionic Distribution and Selectivity of Ionic Liquids in Microporous Electrodes

Justin N. Neal,[1] David J. Wesolowski,[2] Douglas Henderson,[3] and Jianzhong Wu[a)1]

[1)] *Department of Chemical and Environmental Engineering, University of California, Riverside, California 92521*

[2)] *Chemistry Division, Oak Ridge National Laboratory, Oak Ridge, Tennessee 37830*

[3)] *Department of Chemistry and Biochemistry, Brigham Young University, Provo, Utah 84602*

The energy density of an electric double layer capacitor, also known as supercapacitor, depends on ion distributions in the micropores of its electrodes. Herein we study ion selectivity and partitioning of symmetric, asymmetric and mixed ionic liquids among different pores using the classical density functional theory. We find that a charged micropore in contact with mixed ions of the same valence is always selective to the smaller ions, and the ion selectivity, which is strongest when the pore size is comparable to the ion diameters, drastically falls as the pore size increases. The partitioning behavior in ionic liquids is fundamentally different from those corresponding to ion distributions in aqueous systems whereby the ion selectivity is dominated by the surface energy and entropic effects insensitive to the degree of confinement.

Keywords: porous electrodes, ion selectivity, classical density functional theory

---

[a)] Corresponding author. E-mail: jwu@engr.ucr.edu

I. INTRODUCTION

The properties of ionic fluids in nanopores underpin some of the most interesting and vital phenomena that are important in diverse fields of electrochemistry and biophysics, from ion channels[1] to advanced carbon electrodes for energy conversion and storage[2]. Ion transport in micropores are commonplace not only in electrochemical devices[3] but also within the soil as well as deep within the Earth's crust that are important for the fundamental studies of geochemistry and environmental remediation[4]. In this work, we are interested in energy storage using ionic liquids in nanoporous electrodes. Specifically, we are concerned with the performance of electric double layer capacitors (EDLC), also known as supercapacitors, in terms of both the power density and the energy density.

In essence, a supercapacitor consists of an electrolyte infiltrating in the micropores of electrodes. The energy storage density is primarily determined by the structure of the electric double layer (EDL), i.e., ion distributions within micropores at a given surface electrical potential. According to the conventional model of electrochemistry, the EDL can be divided into the Stern layer and the diffuse layer: the former is a densely packed structure dictated by irreversible chemical binding; and the latter consists of ions of mainly opposite charge to the applied surface potential. Because irreversible bindings of chemical species to the electrodes are considered as adverse effects, the EDLC performance is dominated by electro-physical adsorption of ionic species in the micropores. The EDL structure depends not only on the composition of the ionic species in the bulk but also on the applied surface potential and the morphology of porous electrodes.

Commercial EDLCs mostly employ porous carbons as the electrodes. The carbon-based material has the benefits of being less expensive yet highly conductive as well as having large specific surface areas. The carbide-derived carbon is one such material recently developed and has an added benefit of a tunable pore size distribution[2]. Because both the power density and the energy density are proportional to the specific surface area, the larger the surface area for a specific electrode material, the greater the energy storage capacity. Among various electrolytes for EDLCs, organic electrolytes (e.g., propylene carbonate and acetonitrile) and room-temperature ionic liquids (RTILs) are often preferred over aqueous electrolytes due to their wider operating potential windows. In particular, ionic liquids are commonly adopted in research labs because of excellent thermal stability and non-volatility.

Understanding ion partitioning between the micropores of porous electrodes and the bulk electrolyte and ion distribution within different pores represents a key step toward gaining fundamental knowledge to increase the efficiency and capacity of EDLCs for energy storage. While the electrolyte composition in the bulk can be precisely controlled, relatively little is known on the microscopic details of the electrodes such as the morphology and chemical structure of individual micropores. Such information is instrumental to determine the EDL structure from a molecular perspective. Because direct measurement of the density profiles of ionic liquids near a surface or within porous electrodes is difficult with experimental methods, the ionic distributions are conventionally described with various EDL models or molecular simulations[5,6]. As demonstrated by Blum and coworkers[7], the essential physics of ionic systems can be reasonably described by the primitive model that accounts for the electrical charges and the diameters of the ionic species in a dielectric background. A similar approach has been successfully applied to EDL systems[8].

Previous work on ion distribution in small pores has been mostly concerned with aqueous solutions[5,9,10]. In particular, a hard-sphere model was used to study the partitioning of various ions between micropores and an aqueous electrolyte solution using the classical density functional theory (cDFT)[11]. It was found that the "entropic effect" dominates ion selectivity, i.e., surface attraction makes the pore to be more selective to smaller ions while solvent depletion leads to the selection of larger ions. Interestingly, the charge-space competition of ionic species can be successfully described without explicit consideration of the surface charge or ionic distributions inside the pore[12].

The properties of an ionic liquid can be substantially different from those corresponding to an aqueous electrolyte solution not only in terms of the increased strength of electrostatic interactions due to the lack of a dielectric medium but also in terms of the high packing densities of ionic species. As shown in previous experimental and theoretical studies[8,13,14], an ionic liquid in contact with a highly charged surface is able to form lamellar structure with alternating layers of cations and anions. While numerous theoretical investigations have been devoted to understanding ion partitioning between aqueous solutions and nanopores, much less is known for EDL systems containing ionic liquid mixtures.

II. METHODS

We consider an ionic liquid in equilibrium with the micropores of a carbon electrode typically used for EDLC applications. As shown schematically in Figure 1, the ionic system is represented by the primitive model of electrolytes in slit pores. Although the coarse-grained model lacks chemical details, we demonstrated in previous work that it is able to capture both the "bell" to the "camel" shapes in the differential capacitance curve[15], the layer-by-layer distribution of ionic species near highly charged surfaces[8], and an anomalous increase of capacitance for electrodes with very narrow pores[16]. Importantly, the primitive model accounts for electrostatic correlations and ionic excluded volume effects that are ignored in conventional electrochemical theories (e.g., the Poisson—Boltzmann equation) and allows for easy variation of the wall potential and the mixture composition[17].

To make our theoretical calculations relevant to experimental systems, we select the parameters such that the ionic model approximately mimics cations and anions commonly used for EDLCs. Specifically, the systems discussed in this work consist of two anions of the same valence but different sizes, representing tetrafluoroborate (BF_4^-) and bis(trifluoro-methylsulfonyl)imide ($TFSI^-$), and one common cation representing 1-ethyl-3-methylimidazolium ($EMIm^+$). EMIm-TFSI and EMIm-BF_4 are two room-temperature ionic liquids widely used in electrochemical devices[18]. Throughout this work, the diameter of the cation ($EMIm^+$) is $\sigma_+ = 0.50\ nm$, and those for two anions (BF_4^- and $TFSI^-$) are $0.30\ nm$ and $0.50\ nm$, respectively. These ion diameters were chosen to account for the excluded volume effects and have been successfully used in previous studies of EDLC.[16,19] For all systems considered in this work, we fix the total number density of ionic species in the bulk at $4.64\ nm^{-3}$, which corresponds to 3.84 M or 259 cm^3/mol for pure EMIm-TFSI at 298 K and 1 bar. While mixing the two ionic liquids at the constant total number density may lead to an unreasonable pressure for the bulk phase, we fix the cation density in all mixtures for convenience. The pressure effect on the excess chemical potential of an ionic liquid is insignificant because of the negligible excess partial molar volume of ionic species. The volume of mixing for ionic liquid mixtures is very small, typically less than 0.1% of the overall volume[20]. A much larger total ion density in the bulk ($7.78\ nm^{-3}$, corresponding to pure EMIm-BF_4 at 298 K and 1 bar) was considered but did not affect the main conclusions of this study.

FIG. 1: A schematic picture of ionic-liquid mixtures considered in this work. Both cations and anions are modeled as spherical particles of different sizes, and the micropores of the amorphous electrode are represented by slit pores. A potential (Φ) is applied to the electrode surface, resulting in an induced surface charge (Q) due to the formation of electric double layer.

Within the primitive model, the pair potential (u_{ij}) between ionic species is given by a hard-core plus Coulombic interaction

$$u_{ij}(r) = \begin{cases} \infty & r < \frac{\sigma_i+\sigma_j}{2} \\ \frac{Z_i Z_j e^2}{4\pi\varepsilon_0 r} & r \geq \frac{\sigma_i+\sigma_j}{2} \end{cases} \tag{1}$$

where r is the center-to-center distance, e is the unit charge, ε_0 is the permittivity of free space, and σ_i and Z_i are the diameter and valence of species i. The primitive model assumes that van der Waals forces, including the effect of ion polarizability, play only a minor role in predicting the thermodynamic properties of electrolyte systems. Because all species in the ionic system are explicitly in this work, the relative dielectric permittivity is set to that of the vacuum ($\varepsilon = 1$). We note that the dielectric relaxation due to ion polarizability may lead to an effective dielectric constant different from unity.

The slit pore model is used to represent porous electrodes as in our previous investigations[16,19]. Each ionic species inside a slit pore experiences an electrical potential due to the surface charge:

$$\beta V_i(z) = \begin{cases} -2\pi l_B Z_i H Q/e, & \frac{\sigma_i}{2} \leq z \leq H - \frac{\sigma_i}{2} \\ \infty, & \text{otherwise} \end{cases} \tag{2}$$

where z is the perpendicular distance from the lower surface, $\beta = 1/(k_B T)$, k_B is the Boltzmann constant, T is temperature, $l_B = \beta e^2/(4\pi\epsilon_0)$ denotes the Bjerrum length, Q represents the surface charge density, and H is the surface-to-surface separation (*viz.*, the pore width). Throughout this work, the Bjerrum length is taken as 55.69 nm, a value corresponding to electrostatic interactions in a vacuum at room temperature. Since the dielectric constant of amorphous carbons is not much different from that of an ionic liquid, we assume that the polarizability of the electrode has relatively small effects on ionic distributions.

The density profiles of ionic species in different pores can be predicted with the classical density functional theory (cDFT)[8]. At a given temperature (T) and the number densities of ionic species in the bulk (ρ_i^0), the density profile for each species (i) is given by

$$\rho_i(z) = \rho_i^0 exp[-\beta V_i^{ex}(z) - \beta Z_i e\Phi(z) - \beta\Delta\mu_i^{ex}(z)] \quad (3)$$

where $V_i^{ex}(z)$ is the non-electrostatic component of the external potential given by Eq.(2), i.e., the potential due to the slit walls that confine the ionic species inside the pore, and $\Delta\mu_i^{ex}(z)$ is the excess chemical potential. The electrostatic part of the external potential is accounted for in the overall local electrical potential, $\Phi(z)$, which is related to the local charge density by the Poisson equation:

$$\frac{\partial^2\Phi(z)}{\partial z^2} = -\frac{e}{\varepsilon_0\varepsilon}\sum_i Z_i\rho_i(z) \quad (4)$$

The last term in Eq.(3) accounts for the thermodynamic non-ideality due to electrostatic correlations and the excluded volume effects. The theoretical performance of the cDFT has been repeatedly calibrated with molecular simulations.[21–24] The detailed expression for the excess chemical potential μ_i^{ex} can be found in our previous work. Without the excess chemical potential, cDFT is reduced to the conventional Poisson—Boltzmann equations.

The density profiles, along with the Poisson equation, can be solved self-consistently with appropriate boundary conditions. The numerical details for cDFT, as well as the analytical expression for the excess chemical potential have been reported in our previous publications[15]. From the density profiles, we can determine the ion selectivity (α),

$$\alpha = \left(\frac{\bar{\rho}_{BF_4}^{pore}}{\rho_{BF_4}^0}\right) \cdot \left(\frac{\bar{\rho}_{TFSI}^{pore}}{\rho_{TFSI}^0}\right)^{-1} \quad (5)$$

The excess absorption (Γ), which provides a direct measurement of ion partitioning, is defined by the difference between the average density of a species (i) within the pore and that of the same species in the bulk:

$$\Gamma_i = \frac{1}{H}\int_0^H [\rho_i(z) - \rho_i^0]dz = \bar{\rho}_i - \rho_i^0 \quad (6)$$

where H represents the pore width, and $\bar{\rho}_i$ stands for the average density inside the pore.

Ion distribution in porous electrodes depends on a range of parameters including the surface potential, electrolyte composition, and the pore sizes. In this particular work, we consider ion partitioning in three slit pores to represent different levels of confinement: the narrow pore (0.80 nm), the intermediate pore that allows for developing layered ionic structures (1.18 nm), and finally a large pore for the fully developed layered structure (2.67 nm). The narrow and large pores (0.80 nm and 2.67 nm) correspond approximately to the two average pore sizes of carbide-derived-carbon (Mo_2C) obtained from gas sorption analysis[18]. Mo_2C exhibits a bimodal pore size distribution.

III. RESULTS AND DISCUSSION

cDFT predicts the density profiles of ionic species in slit pores as a function of the mixture composition, the surface potential, and the pore width. From the ionic densities, we can readily calculate the surface excess for each ion and ion selectivity as well as the capacitance of individual pores. While the EDL capacitance is of tremendous importance for energy storage, our investigation in this work is focused on ion partitioning and distribution in individual pores. As different pores in the same material are uncorrelated according to the slit-pore model (except sharing the same chemical potentials of ionic species in the bulk), studies on the ionic behavior in individual pores provide useful insights on their relative distributions among different pores within a realistic porous electrode. The computational efficiency of cDFT enables us to investigate all pertinent parameters systematically such that we can attain a generic understanding of various forces dictating ion partitioning between the bulk and different pores and the pore selectivity of different ionic species.

A. *Ionic distributions*

We first consider the ionic density profiles in slit pores coexisting with three bulk ionic liquids: EMIm-TFSI, EMIm-BF_4, and their equal molar mixture. Within our coarse-grained model, EMIm-TFSI is represented as a symmetric electrolyte as in the restrictive primitive model often adopted in the literature. EMIm-BF_4 represents an asymmetric electrolyte where the anions are significantly smaller than the cations. The mixture contains two anions of different sizes but with the same bulk concentration. To gain a understanding of the competition between the surface attraction and size effects, we fix the surface electrostatic potential constant (Φ=1.50 V).

1. *Narrow pores*

Figure 2 presents the ion distributions in a narrow slit pore ($H = 0.80$ nm). Here the pore width is only slightly larger than the diameter of large ions (0.50 nm). Because of the spatial restriction, cations and anions are not able to form a multilayer structure in the narrow pore as typical for an ionic liquid near a strongly charged surface. Nevertheless, for all cases, the pore is able to accommodate two layers of counterions (*viz.*, anions) in contact with walls. A layer of coions (*viz.*, cations) is sandwiched between the two counterion layers to alleviate the electrostatic repulsion.

At the same bulk density, the ionic distributions for the symmetric and asymmetric ionic liquids are noticeably different not only in terms of the position and magnitude of the contact density but also in terms of the counterion distribution in the middle of the pore. While cations and anions remain significantly mixed throughout the pore for the symmetric system, they are well segregated as the smaller counterions (BF_4^-) are densely accumulated at the surface. The charge segregation is similar to that was previously found for electrolytes confined in a highly-charged spherical pore[25]. The smaller anions have much larger contact density because they interact more strongly with the surface in addition to being smaller in excluded volumes. Because charge neutrality is preserved for the entire pore, virtually no small anions are found in the middle of the pore for the asymmetric system.

For the slit pore in equilibrium with the ionic liquid mixture containing two types of anions at the the same composition, the slit pore prefers adsorption of the smaller anions that have the opposite charge. While the contact density for the larger counterions is drastically reduced — by almost three orders of magnitude in comparison with that for the symmetric case, the contact density of the smaller ions is virtually independent of the bulk concentration, suggesting that counterion distribution inside the pore is dominated by the surface attraction. The dominance of electrostatic effects is also evident from the close local densities of large and small anions at positions that both are accessible. The enrichment of smaller counterions effectively decreases the EDL thickness, which is important for EDLC applications because a smaller EDL thickness corresponds to a larger capacitance and, consequently, a higher energy storage density.

Figure 2 shows that the density of the coions increases as the counterions become smaller (note the logarithm scale and see Figure 6 below). The increase in the coion concentration

FIG. 2: The ionic density profiles in a narrow slit pore ($H = 0.80\ nm$) in contact with a bulk ionic liquid. In all cases, the surface potential (Φ) is fixed at 1.50 V and the total ion density in the bulk is 4.64 nm^{-3}. The fraction of smaller anions (BF_4^-) in the bulk (x) is, from top to bottom, 0.00, 0.50, and 1.00 respectively.

inside the pore reflects not only a smaller excluded volume of counterions but also a stronger electrostatic pairing energy.

2. Intermediate pore size

To get a more comprehensive understanding of the ionic distributions, we consider the three ionic liquids in larger pores such that multiple layering of the ionic species is allowed. Figure 3 shows that, at an intermediate pore width ($H = 1.18\ nm$), the presence of smaller anions promotes formation of the multilayer structure (*i.e.*, a weak layer of counterions is formed at the middle). Whereas the contact densities are nearly independent of the pore width for both symmetric and asymmetric ionic liquids, for the ionic liquid mixture, the contact density of larger anions in the intermediate pore ($\sim 10\ nm^{-3}$) is higher than that in the narrow pore ($\sim 0.01\ nm^{-3}$) by almost three orders of magnitude. The striking increase in the contact density for larger counterions can be attributed to more efficient packing for particles of different sizes in comparison to those for uniform size when the space is permitted. Because the density profile of the smaller counterions is not changed much by the presence of larger counterions, the application of an ionic liquid mixture is expected to enhance the surface charge density thereby the EDL performance[26].

Interestingly, the coion concentration is nearly uniform in the slit pore of intermediate size, which is in striking contrast to the parabolic shape shown in Figure 2 for the narrow pore and to the oscillatory distributions in larger pores (see Figure 4 below). The uniform coion distribution reflects the competing contributions from the excluded volume effects and electrostatic interactions. While counterions are attracted to the pore primarily due to the surface attraction, formation of a weak layer of counterions at the middle reduces electrostatic repulsion among the coions. Unlike that in a narrow pore, the multilayer formation makes the counterion distribution at the pore center strongly dependent on its

FIG. 3: Similar to Figure 2 but in an intermediate size pore ($H = 1.18\ nm$).

FIG. 4: The ionic liquid density profile is shown for a large pore ($H = 2.67\ nm$), with all else the same as Figure 2.

size.

3. Large pores

As the pore size further increases, the ionic distribution near the electrode surface exhibits the characteristic layer-by-layer structure[8]. For a symmetric ionic liquid, the multilayer structure can extend up to ten times the hard-core diameter, manifesting long-range electrostatic correlations in an ionic system. The range of correlation is substantially reduced for an asymmetric electrolyte system because of more efficient packing and intercalating of particles of different sizes[27].

Figure 4 shows that, except the multilayer structures, the ion distributions in a large slit pore ($H = 2.67\ nm$) are not much different from those in the intermediate pore. For all cases, the contact densities are virtually independent of the pore size, signaling the surface saturation effect.

B. *Ion selectivity*

As one may deduce from the ionic density profiles discussed above, for counterions of the same valence, smaller counterions are always preferred over larger ones by a highly charged slit pore. However, less obvious is how ion selectivity α, as defined by Equation 5, changes with the pore size and the bulk concentration. For nanopores in contact with an aqueous electrolyte, a previous study indicates that ion selectivity is mainly determined by the surface energy and entropic effects, little influenced by the pore size[11]. Because solvent molecules play a major role in ion distributions, we expect that the physics underlying ion selectivity in ionic liquids will be very different from that in aqueous systems.

In the following, we investigate systematically ion adsorption and selectivity for the three ionic liquid mixtures mentioned above in narrow, intermediate, and large pores over a broad

FIG. 5: Ion selectivity (α) *vs.* the bulk composition of anions for ionic liquid mixtures in three representative slit pores. The pore widths are $H = 0.80$, 1.18 and 2.67 nm. In all cases, the surface potential (Φ) is fixed at 1.50 V. The selectivity for the smaller counterions is the largest for the narrow pore. As the pore size increases, the slit pore remains selective to the smaller anions but the selectivity is drastically reduced.

range of surface potentials and bulk compositions. As a reminder, BF_4^- is referred to as the smaller anion ($\sigma_{BF_4} = 0.30\ nm$) throughout this work, and TFSI^- ($\sigma_{TFSI} = 0.50\ nm$) is the larger anion. So for $\alpha > 1$, a pore is small anion selective; and for $1 > \alpha > 0$, the pore is large anion selective.

1. Ion selectivity and partitioning

Figure 5 shows that a narrow pore ($H = 0.80\ nm$ and $\Phi = 1.50\ V$) is extremely selective to smaller anions when the surface is positively charged. The large ion selectivity reflects near complete depletion of larger anions inside the pore as shown in Figure 2. The small ion selectivity is enhanced as its molar fraction in the bulk increases, suggesting that the narrow pore is tightly packed with the small counterions. The concentration effect shows opposite trends for larger pores because significant amount of larger cations can be accommodated in direct contact with the surface. In other words, larger pores allow formation of a "composite" Helmholtz layer that provides more efficient packing of the counterions and such composite structure is prohibited in the narrow pore.

In stark contrast to aqueous systems[11], the ion selectivity is extremely sensitive to the pore size. The pore size effect is most dramatic for the dilute mixtures of lager counterions. The size effect is less of an issue for aqueous systems because the packing density of ionic species is much smaller. In the absence of solvent molecules, the micropores always prefer adsorption of smaller counterions from an ionic liquid mixture.

Ion partitioning between the bulk and the confined space is directly related to the surface excess Γ as defined by Equation 6. If $\Gamma > 0$, the ions prefer adsorption inside the pore; and otherwise if $\Gamma < 0$. As shown in Figure 6, both the smaller anions and the cations become enriched inside the pore whereas the larger anions are depleted as the concentration

FIG. 6: The surface excesses for different ions adsorption in a narrow slit pore ($H = 0.80$ nm). Here the surface potential (Φ) is 1.50 V.

FIG. 7: The same as Figure 6 but for $H = 1.18$ nm

of the smaller anion in the bulk increases. For this particular case, the average density of the coions in the pore is almost the same as the bulk value for the symmetric ionic liquid (in the absence of BF_4, $x = 0$). Because of the saturation effects, the surface excess shows a maximum for the smaller counterions and a minimum for the larger counterions at the same bulk composition. The reduction (increase) of the surface excess for the smaller (larger) anions is mainly due to the increase (decrease) in the bulk density.

Figures 7 and 8 show that the surface excess for the smaller counterions is reduced as the pore size increases. Meanwhile, the larger counterions are less depleted from the pore. In all cases, the surface excess is always positive for the coions, implying charge reversal inside the pore due to the overcompensation of the surface charge. Like that for the smaller counterions, the adsorption of coions falls as the pore size increases. Because the concentration of the coions in the bulk is fixed, its surface excess is relatively insensitive to the counterion composition beyond the surface saturation.

2. The effect of surface potential

The conventional wisdom for ion selectivity is that smaller ions are selected because of their larger surface potential. In the absence of energetic forces, larger particles are always preferred inside the pore due to entropic effects related to the particle excluded volume. While such understanding is consistent with above discussions for anion adsorption in positively charged pores, we find that smaller ions can also be selected by the pores even when the surface energy is more repulsive. Figure 9 shows the selectivity of the smaller anions (BF_4 *vs.* TFSI) by both positively and negatively charged pores over a broad range of the surface potential. A neutral pore is biased to neither smaller nor larger anions because

FIG. 8: The same as Figure 6 but for $H = 2.67$ nm

FIG. 9: The selectivity of BF_4 over TFSI by the three slit pores as a function of the surface potential. Here the molar fraction of the smaller anions is fixed at $x = 0.50$.

of the compensation of size effects and electrostatic interactions. While the entropic effects favor exclusion of larger particles from the bulk, accommodation of smaller ions inside the pore is energetically more favorable.

As expected, the small ion selectivity increases as the surface potential rises. When the surface potential becomes more negative, the adsorption of cations leads to stronger charge reversal and, subsequently, the "effective surface energy" for the smaller anions increases. In other words, the smaller anions are more favorably selected by a negatively charged pore due to their stronger pairing energy with the cations in direct contact with the surface. Similar to that for the positively charged pores, the selectivity falls as the pore size increases. At the same value of the surface potential, the selectivity for smaller ions is stronger when the surface charge is opposite because its adsorption is driven by charge reversal.

IV. CONCLUSIONS

We demonstrate in this work that ion selectivity by the micropores of an electrode in contact with a room-temperature ionic liquid is fundamentally different from that for ion channels or nanopores in aqueous systems that have been extensively studied in the literature. A charged pore in contact with an ionic mixture attracts smaller ions of the same valence not only when the surface bears the opposite charge or stronger attraction but also when it has the same charge exerting a stronger electrostatic repulsion. Unlike entropic effects discussed in an earlier theoretical work[11], ion selectivity is extremely sensitive to the pore size. For an ionic liquid mixture in contact with a highly charged narrow pore with the pore size comparable to the ion diameters, the ion distribution inside the pore is dominated by the close packing of the smaller counterions, and the severe confinement may lead to virtually complete depletion of larger counterions. In this case, the counterions and coions are well segregated inside the pore and the selectivity toward smaller ions rises as its composition in the bulk increases. For the ionic liquid mixture in contact with larger pores that allow the development of layer-by-layer ionic distributions, the pores are also smaller ions selective but the selectivity falls with the smaller ion concentration. In this case, counterions of different sizes are packed more efficiently than single ions, leading to drastic decreases of the selectivity and concentration effects. In addition to fundamental physics, the theoretical results provide useful insights into the design and selection of ionic liquid mixtures and porous electrodes for electric double layer capacitors and for understanding ionic separation processes.

ACKNOWLEDGEMENTS

This research was sponsored by the Fluid Interface Reactions, Structures and Transport (FIRST) Center, an Energy Frontier Research Center funded by the U.S. Department of Energy, Office of Science, Office of Basic Energy Sciences. The numerical calculations were performed at the National Energy Research Scientific Computing Center (NERSC).

REFERENCES

[1] D. Boda, David D. Busath, Bob Eisenberg, Douglas Henderson, and Wolfgang Nonner, Phys. Chem. Chem. Phys. **4**, 5154 (2002).

[2] P. Simon and Y. Gogotsi, Nat. Mater. **7**, 845 (2008).

[3] J. Maier, Nat. Mater. **4**, 805 (2005).

[4] B. Karn, T. Kuiken, and M. Otto, Environ. Health Perspect. **117**, 1823 (2009).

[5] R. Hayes, G. G. Warr, and R. Atkin, Chem. Rev. **115**, 6357 (2015), pMID: 26028184.

[6] C. Pean, B. Daffos, B. Rotenberg, P. Levitz, M. Haefele, P.-L. Taberna, P. Simon, and M. Salanne, J. Amer. Chem. Soc. **137**, 12627 (2016).

[7] J.-P. Simonin, L. Blum, and P. Turq, J. Phys. Chem. **100**, 7704 (1996).

[8] J. Wu, T. Jiang, D.-E. Jiang, Z. Jin, and D. Henderson, Soft Matter **7**, 11222 (2011).

[9] C.-H. Hou, P. Taboada-Serrano, S. Yiacoumi, and C. Tsouris, J. Chem. Phys. **129**, 224703 (2008).

[10] F. Moucka, D. Bratko, and A. Luzar, J. Chem. Phys. **142**, 124705 (2015).

[11] R. Roth and D. Gillespie, Phys. Rev. Lett. **95**, 247801 (2005).

[12] D. Boda, D. D. Busath, D. Henderson, and S. Sokołowski, J. Phys. Chem. B **104**, 8903 (2000).

[13] Y. Lauw, M. D. Horne, T. Rodopoulos, and F. A. M. Leermakers, Phys. Rev. Lett. **103**, 117801 (2009).

[14] M. Z. Bazant, B. D. Storey, and A. A. Kornyshev, Phys. Rev. Lett. **106**, 046102 (2011).

[15] D.-E. Jiang, D. Meng, and J. Wu, Chem. Phys. Lett. **504**, 153 (2011).

[16] D.-E. Jiang, Z. Jin, and J. Wu, Nano Lett. **11**, 5373 (2011).

[17] D.-E. Jiang, Z. Jin, D. Henderson, and J. Wu, J. Phys. Chem. Lett. **3**, 1727 (2012).

[18] K. L. V. Aken, M. Beidaghi, and Y. Gogotsi, Angew. Chem. Int. Ed. **54**, 4806 (2015).

[19] D. Jiang and J. Wu, J. Phys. Chem. Lett. **4**, 1260 (2013).

[20] H. Niedermeyer, J. P. Hallett, I. J. Villar-Garcia, P. A. Hunt, and T. Welton, Chem. Soc. Rev., 2012, 41, **41**, 7780 (2012).

[21] J. Jiang, D. Cao, D. Henderson, and J. Wu, J. Chem. Phys. **140**, 044714 (2014).

[22] Z. Li and J. Wu, J. Phys. Chem. B **110**, 7473 (2006).

[23] Y.-X. Yu, J. Wu, Y.-X. Xin, and G.-H. Gao, J. Chem. Phys **121**, 1535 (2004).

[24] Z. Li and J. Wu, Phys. Rev. E **70**, 031109 (2004).

[25] J. Yu, L. Degrève, and M. Lozada-Cassou, Phys. Rev. Lett. **79**, 3656 (1997).

[26] C. Lian, K. Liu, K. L. Van Aken, Y. Gogotsi, D. J. Wesolowski, H.L. Liu, D.E. Jiang, and J. Wu, ACS Energy Lett. **1**, 21 (2016).

[27] D. Henderson, W. Silvestre-Alcantara, M. Kaja, S. Lamperski, J. Wu, and L. B. Bhuiyan, J. Mol. Liq. (2016), 10.1016/j.molliq.2016.08.051.

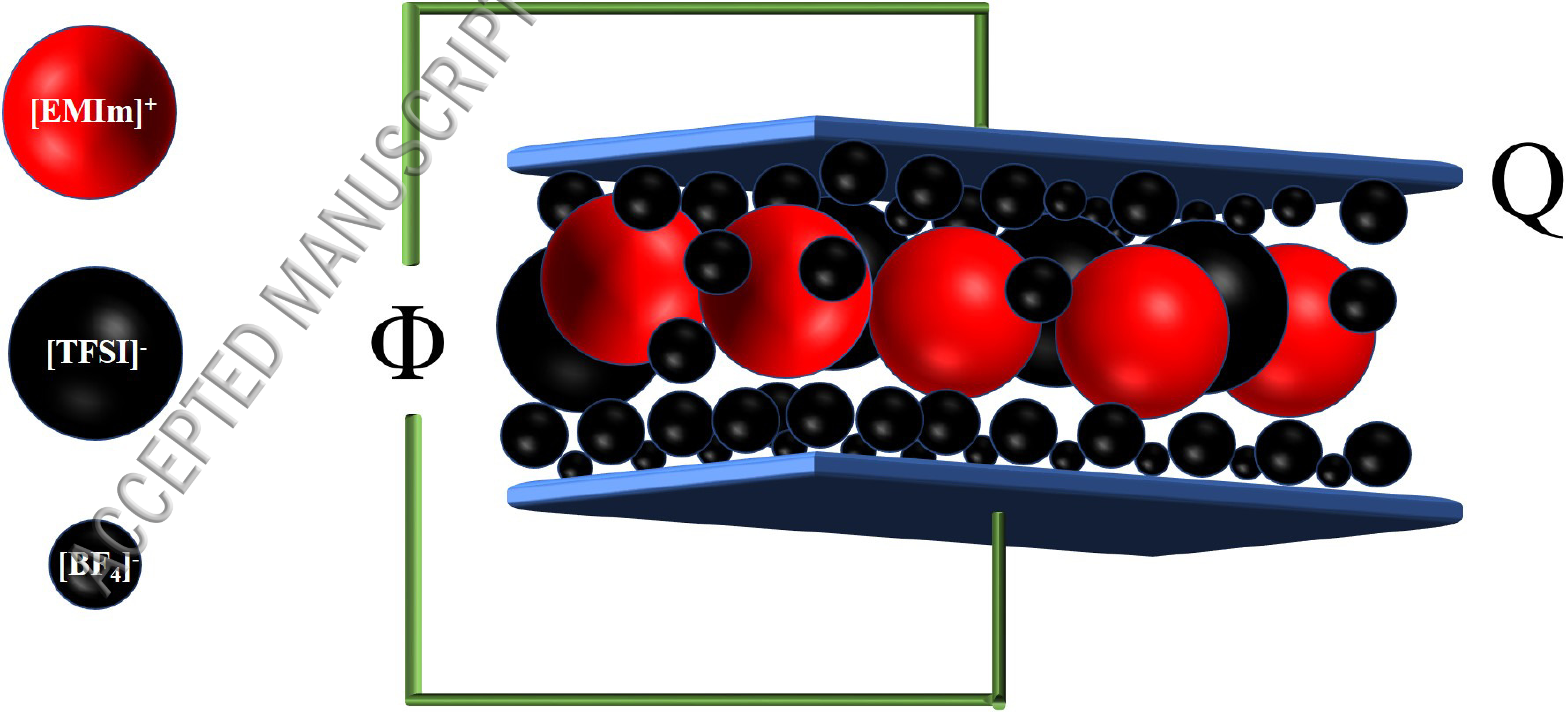
[EMIm]$^+$
[TFSI]$^-$
[BF$_4$]$^-$
Φ
Q

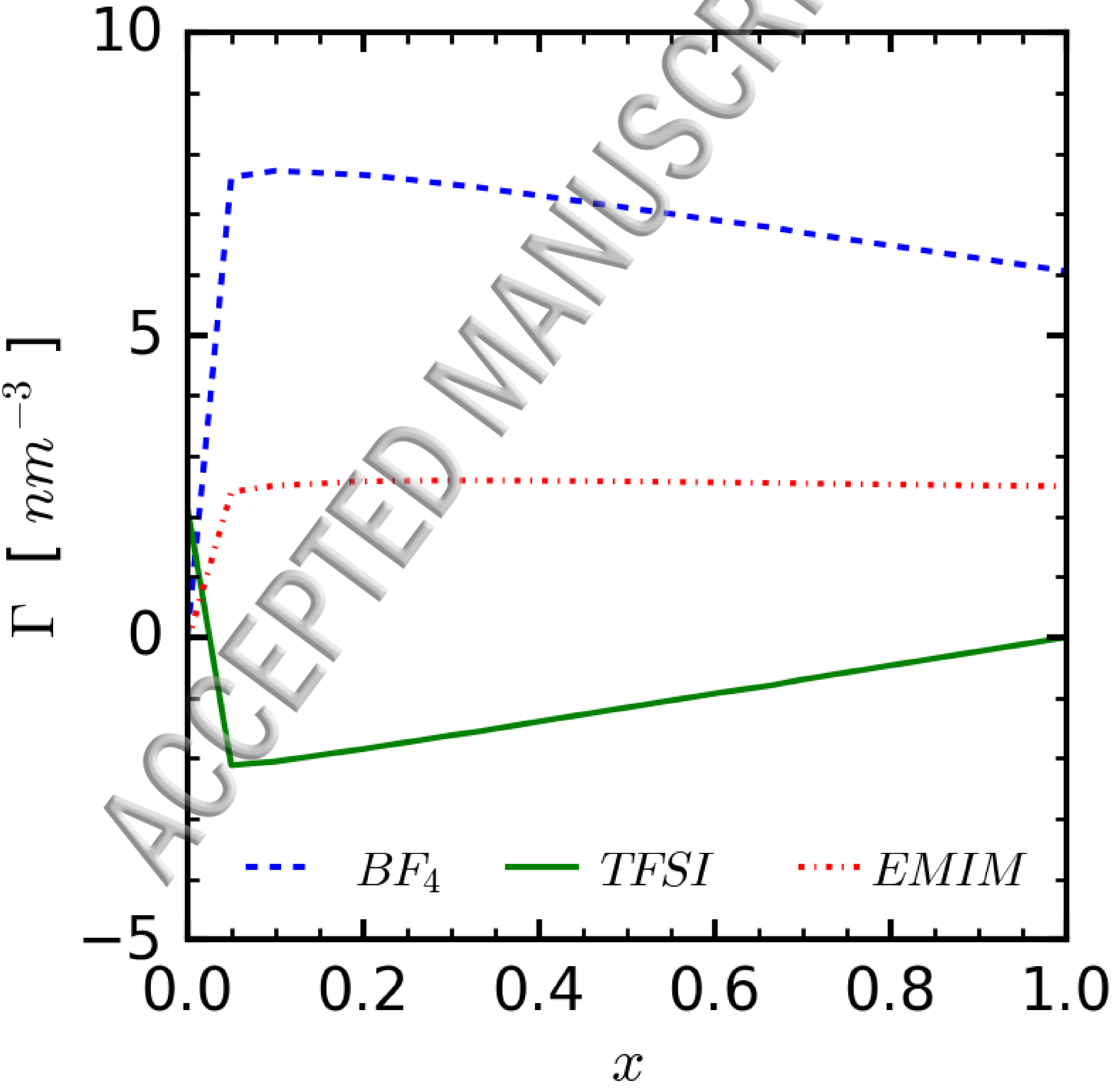
10
5
0
−5
Γ [nm^{-3}]
0.0
0.2
0.4
0.6
0.8
1.0
x
BF_4
$TFSI$
$EMIM$

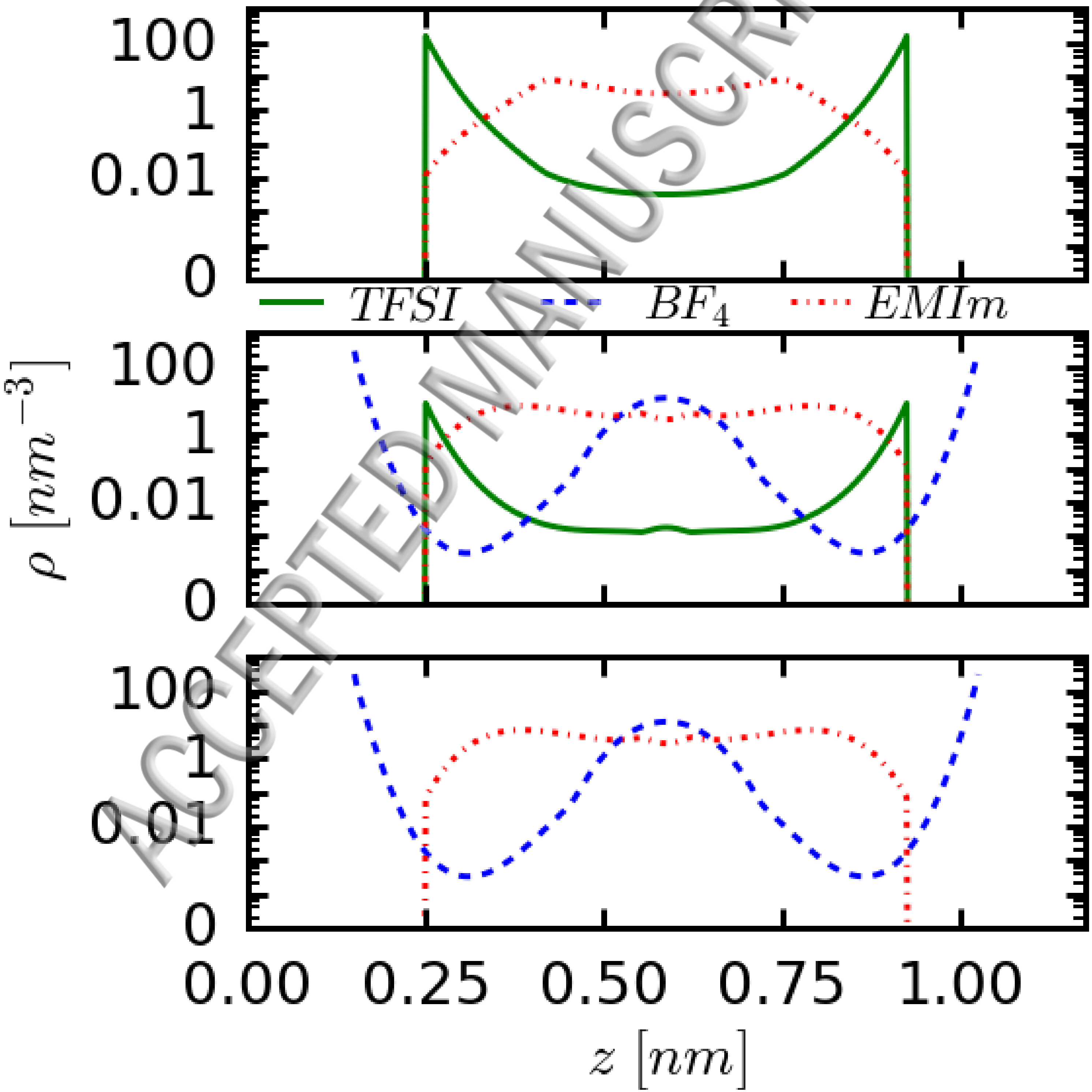
100
1
0.01
0
TFSI
BF$_4$
EMIm
$\rho\ [nm^{-3}]$
0.00
0.25
0.50
0.75
1.00
$z\ [nm]$

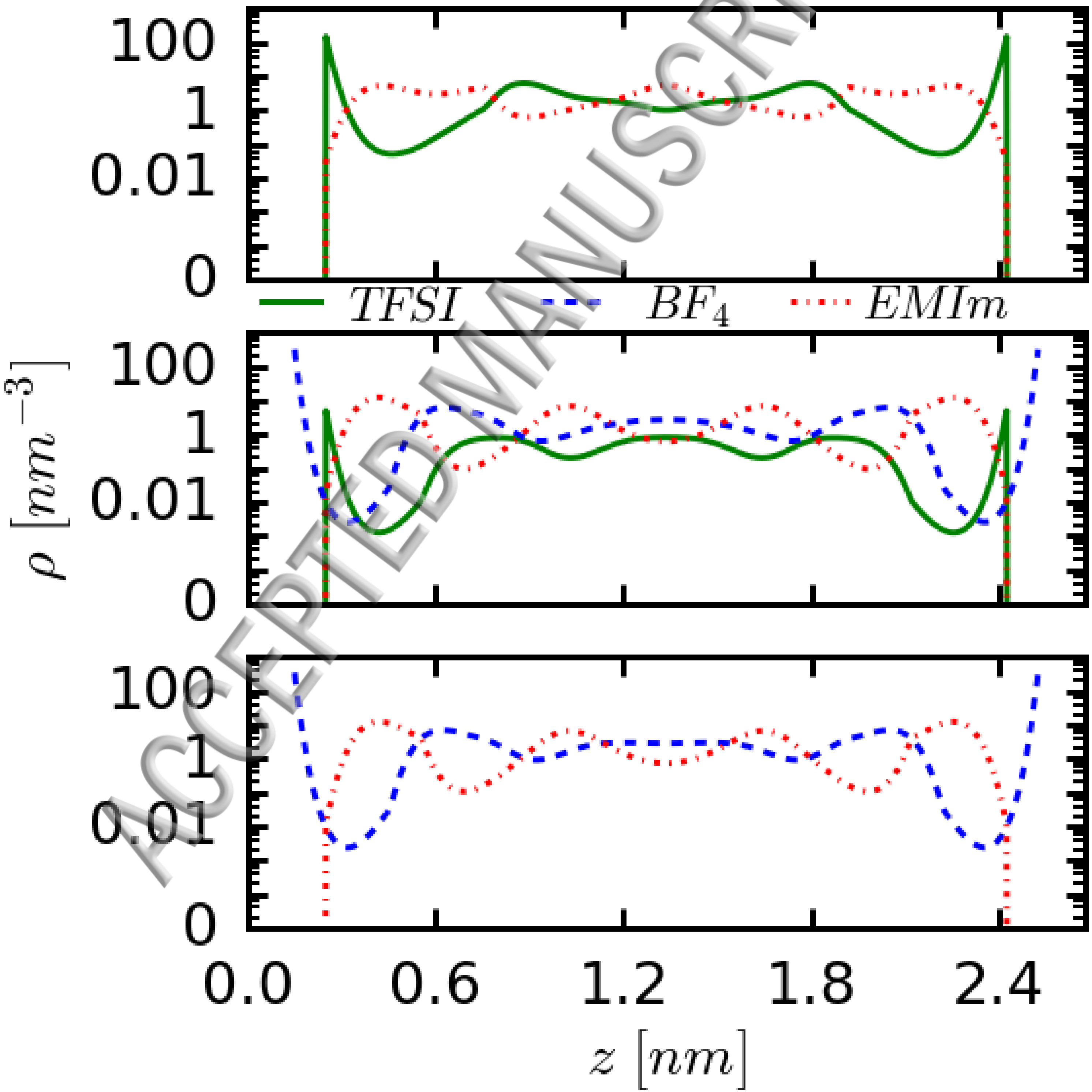
100
1
0.01
0
TFSI
BF_4
EMIm
$\rho\ [nm^{-3}]$
0.0
0.6
1.2
1.8
2.4
$z\ [nm]$

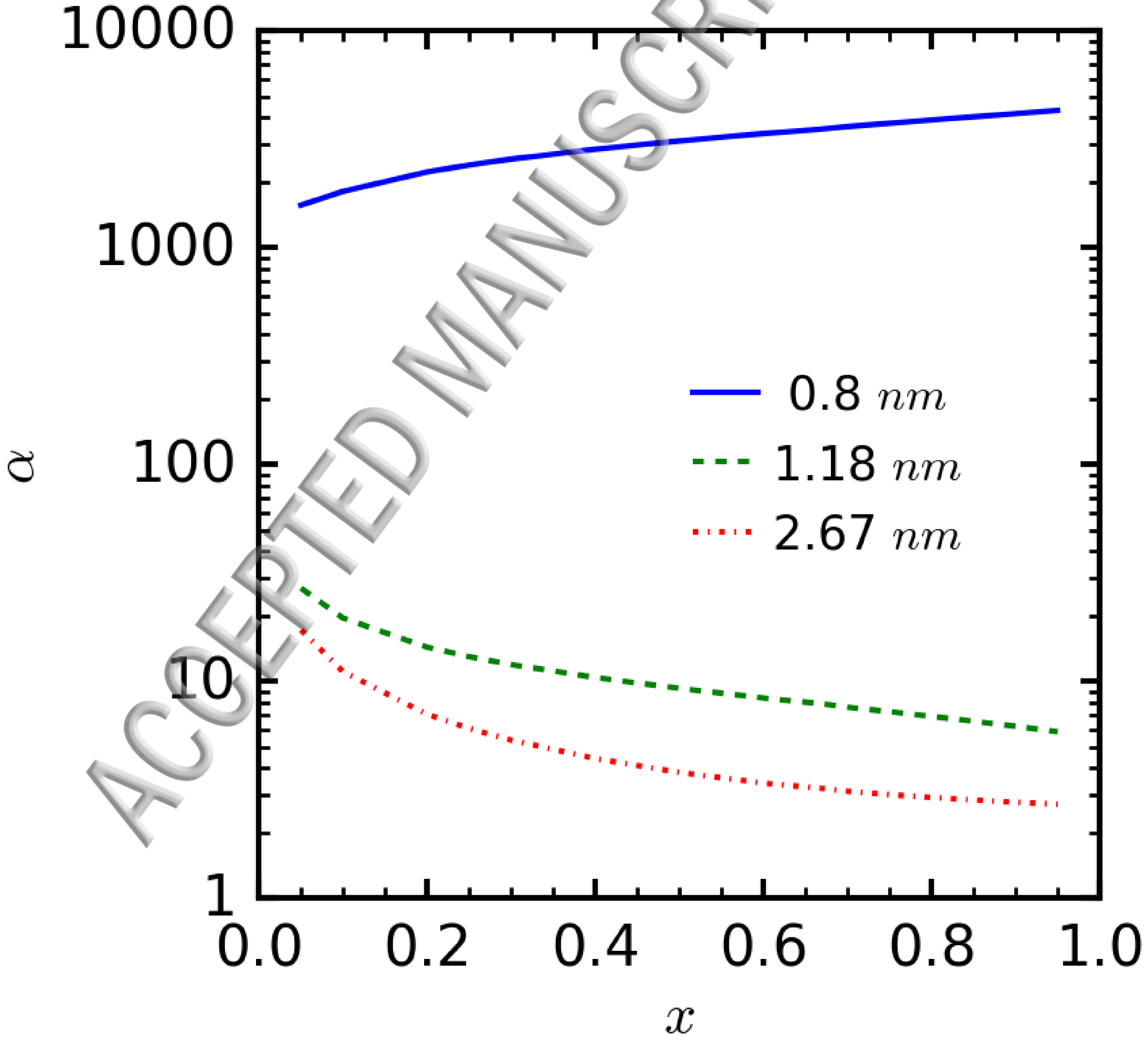
10000
1000
100
10
1
α
0.0
0.2
0.4
0.6
0.8
1.0
x
0.8 nm
1.18 nm
2.67 nm

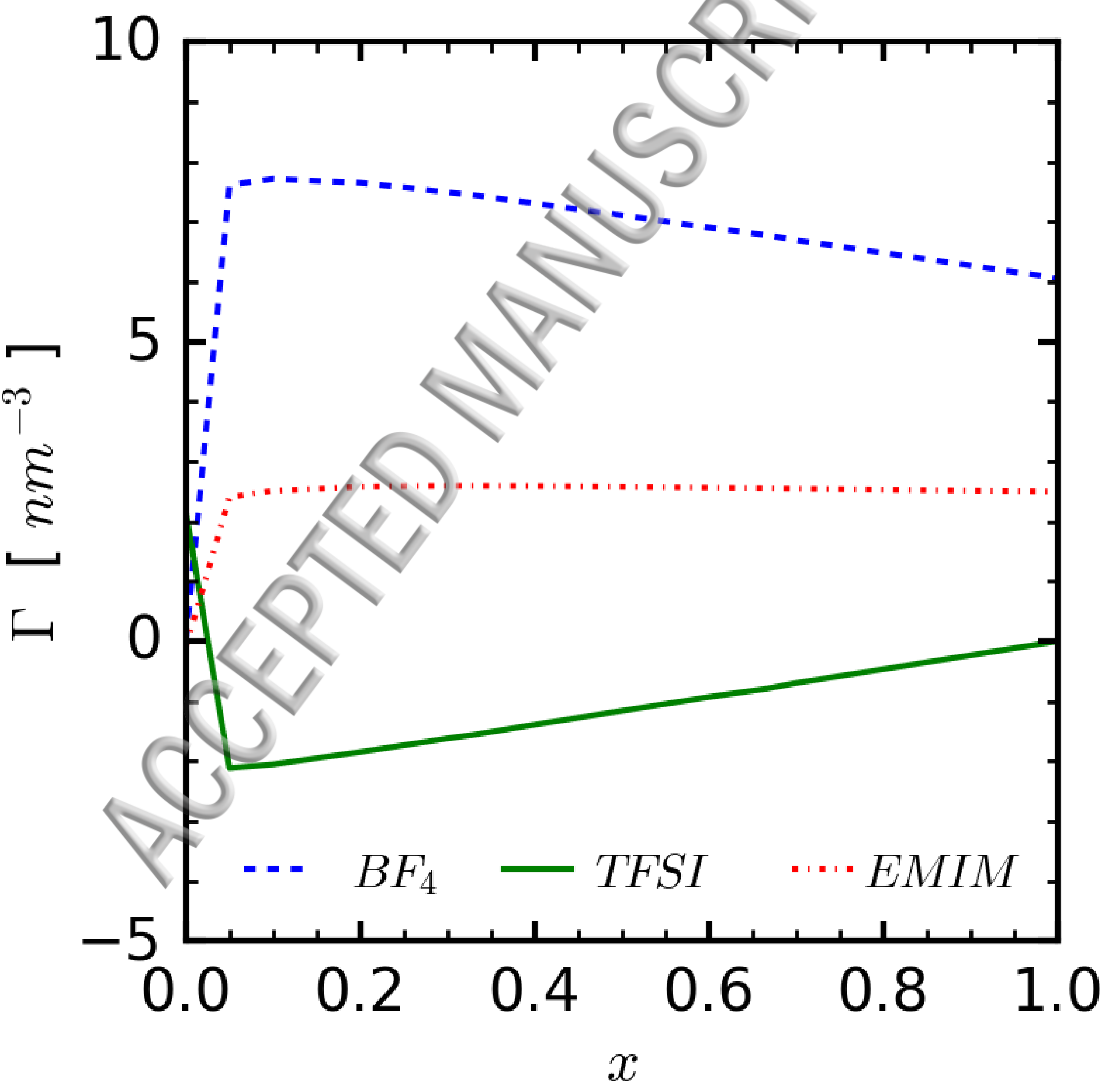
10
5
0
−5
Γ [nm^{-3}]
0.0
0.2
0.4
0.6
0.8
1.0
x
BF_4
$TFSI$
$EMIM$

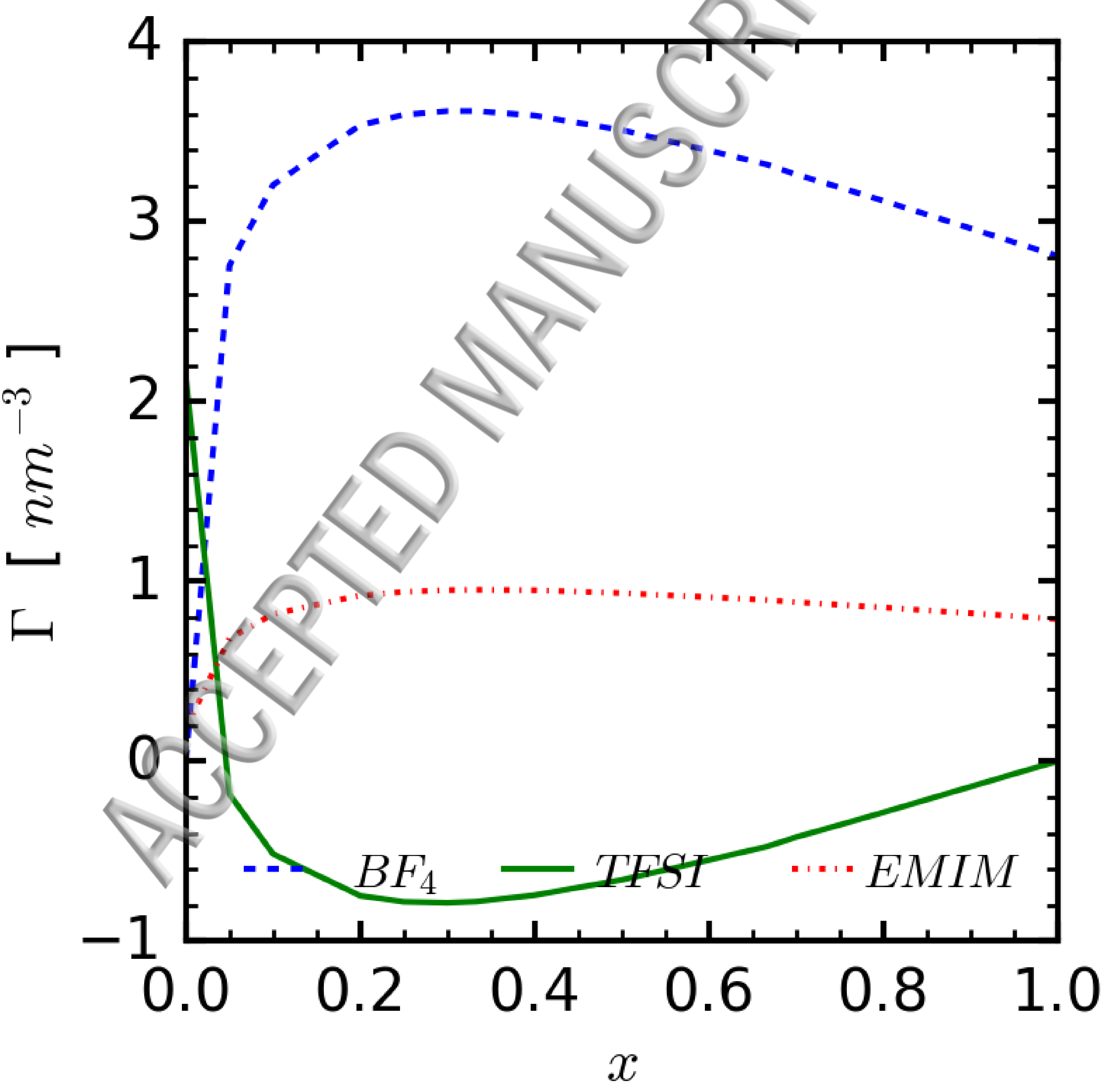

$\Gamma\ [\ nm^{-3}\ ]$
4
3
2
1
0
−1
0.0
0.2
0.4
0.6
0.8
1.0
x
BF_4
$TFSI$
$EMIM$

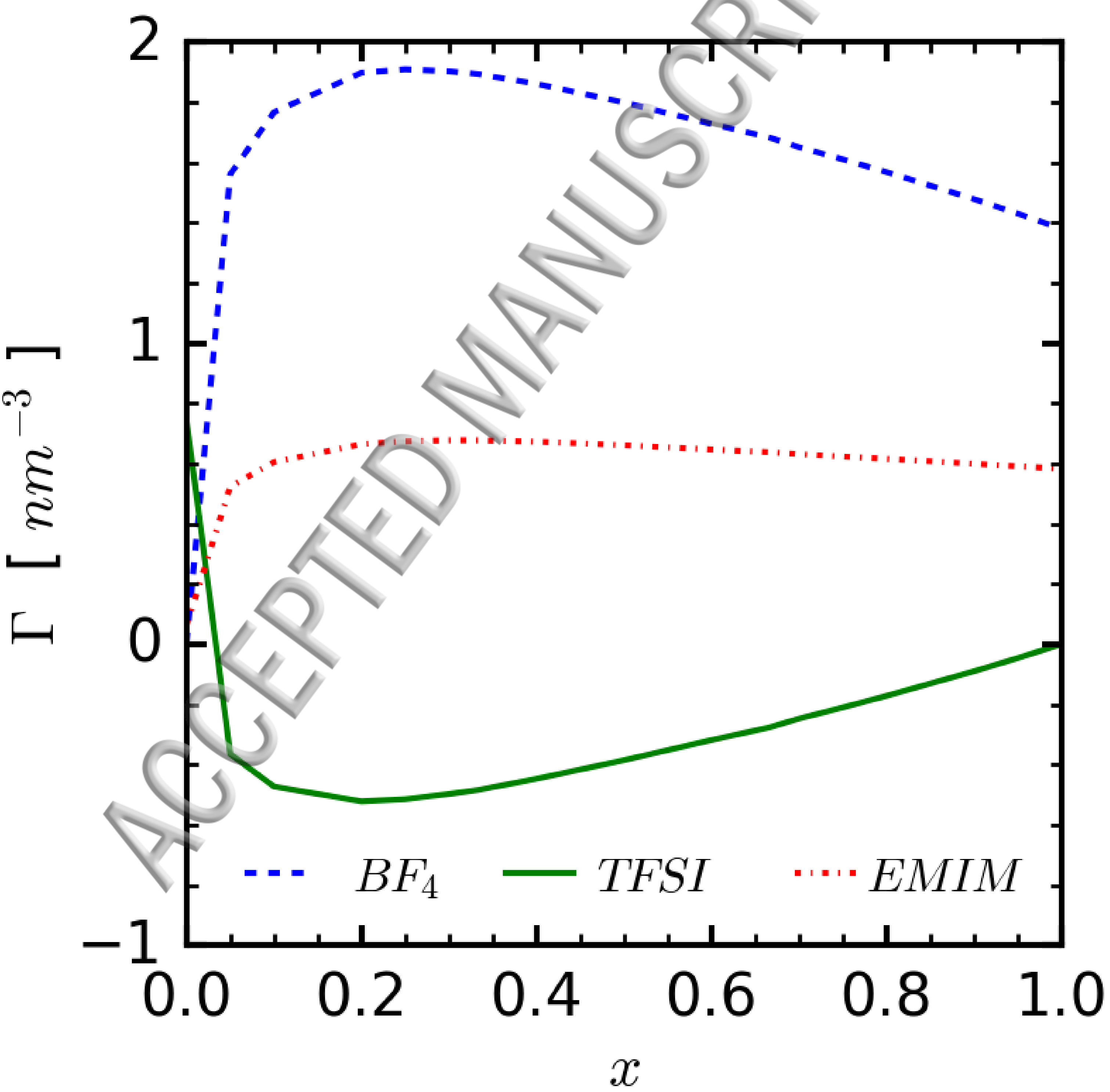

Γ [nm^{-3}]
2
1
0
−1
0.0
0.2
0.4
0.6
0.8
1.0
x
BF_4
$TFSI$
$EMIM$

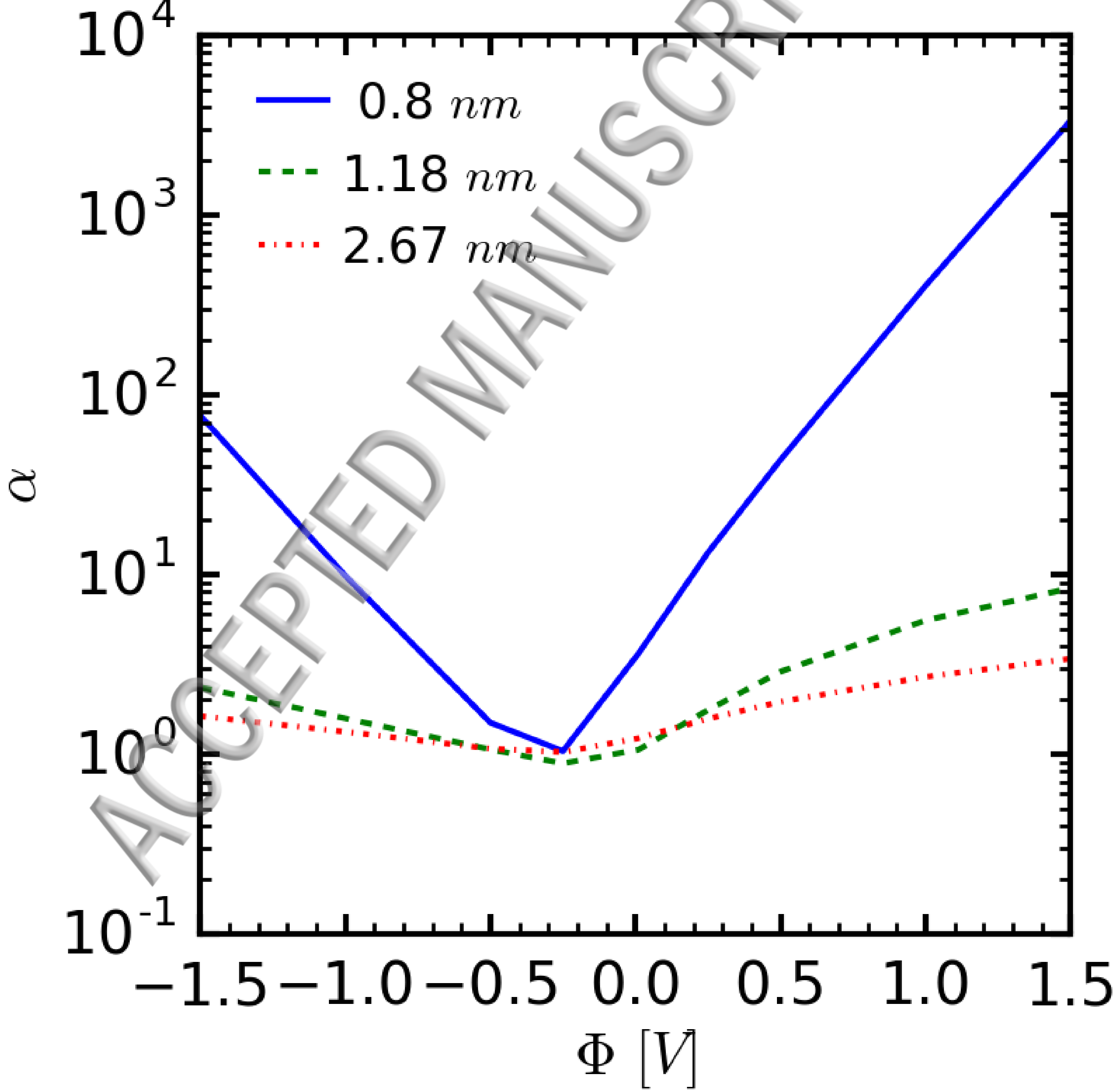
10^4
10^3
10^2
10^1
10^0
10^{-1}
α
0.8 nm
1.18 nm
2.67 nm
−1.5
−1.0
−0.5
0.0
0.5
1.0
1.5
$\Phi\ [V]$